

# Radiopurity of NaI(Tl) crystals for PICOLON dark matter experiment

K. Kotera<sup>\*1</sup>, D. Chernyak<sup>2</sup>, H. Ejiri<sup>3</sup>, K. Fushimi<sup>4</sup>, K. Hata<sup>5</sup>, R. Hazama<sup>6</sup>,  
T. Iida<sup>7</sup>, H. Ikeda<sup>5</sup>, K. Imagawa<sup>8</sup>, K. Inoue<sup>5,9</sup>, H. Ito<sup>10</sup>, T. Kishimoto<sup>11</sup>,  
M. Koga<sup>5,9</sup>, A. Kozlov<sup>12</sup>, K. Nakamura<sup>9,13</sup>, R. Orito<sup>4</sup>, T. Shima<sup>3</sup>,  
Y. Takemoto<sup>9,14</sup>, S. Umehara<sup>3</sup>, Y. Urano<sup>15</sup>, K. Yasuda<sup>8</sup>, and S. Yoshida<sup>14</sup>

<sup>1</sup>*Graduate School of Advanced Technology and Science for Innovation,  
Tokushima University, 2-1 Minami Josanjimacho, Tokushima, Tokushima,  
770-8506, Japan*

*\*E-mail: c612344002@tokushima-u.ac.jp*

<sup>2</sup>*Department of Physics and Astronomy, University of Alabama, Tuscaloosa,  
AL 35487, USA*

<sup>3</sup>*Research Center for Nuclear Physics, Osaka University, 10-1 Mihogaoka,  
Ibaraki, Osaka, 567-0047, Japan*

<sup>4</sup>*Department of Physics, Tokushima University, Tokushima University, 2-1  
Minami Josanjimacho, Tokushima, Tokushima, 770-8506, Japan*

<sup>5</sup>*Research Center for Neutrino Science, Tohoku University,  
6-3AramakiAzaAoba, Aobaku, Sendai, Miyagi, 980-8578, Japan*

<sup>6</sup>*Department of Environmental Science and Technology, Osaka Sangyo  
University, 3-1-1 Nakagaito, Daito, Osaka, 574-8530, Japan*

<sup>7</sup>*Faculty of Pure and Applied Sciences, University of Tsukuba, 1-1-1  
Tennoudai, Tsukuba, Ibaraki, 305-8571, Japan*

<sup>8</sup>*I.S.C.Lab, 5-15-24 Torikai Honmachi, Settsu, Osaka, 566-0052, Japan*

<sup>9</sup>*Kavli Institute for the Physics and Mathematics of the Universe (WPI),  
5-1-5 Kashiwanoha, Kashiwa, Chiba, 277-8583, Japan*

<sup>10</sup>*Department of Physics, Faculty of Science and Technology, Tokyo  
University of Science, Noda, Chiba 278-8510, Japan*

<sup>11</sup>*Department of Physics, Osaka University, 1-1 Machikaneyama-cho,  
Toyonaka, Osaka, 560-0043, Japan*

<sup>12</sup>*National Research Nuclear University "MEPhI" (Moscow Engineering  
Physics Institute), Moscow, 115409, Russia*

<sup>13</sup>*Butsuryo College of Osaka, 3-33 Ohtori Kitamachi, Nishi ward, Sakai,  
Osaka, 593-8328, Japan*

<sup>14</sup>*Institute of Laser Engineering, Osaka University, 2-6 Yamadaoka, Suita,  
Osaka, 565-0871, Japan*

<sup>15</sup>*Institute for Materials Research, Tohoku University, 2-1-1 Katahira,  
Aobaku, Sendai, Miyagi, 980-8577, Japan*

.....  
The dark matter observation claim by the DAMA/LIBRA collaboration has been a long-standing puzzle within the particle physics community. Efforts of other research groups to verify the claim have been insufficient by significant radioactivity of present NaI(Tl) crystals. PICOLON (Pure Inorganic Crystal Observatory for LOw-energy Neut(ra)lino) experiment conducts independent search for Weakly Interacting Massive Particles (WIMPs) using NaI(Tl) crystals. Our NaI(Tl) crystal manufactured in 2020 (Ingot #85) reached the same purity level as DAMA/LIBRA crystals. In this report, we describe the radiopurity of the new Ingot #94 crystal produced using the same purification technique as Ingot #85. The  $\alpha$ -ray events were selected by pulse-shape discrimination method. The impurities in the Ingot #94,  $^{232}\text{Th}$ ,  $^{226}\text{Ra}$  and  $^{210}\text{Po}$  radioactivity were  $4.6 \pm 1.2 \mu\text{Bq/kg}$ ,  $7.9 \pm 4.4 \mu\text{Bq/kg}$ , and  $19 \pm 6 \mu\text{Bq/kg}$ , which are equivalent to those of the DAMA/LIBRA crystals. The background rate in the energy region of 2–6 keV<sub>ee</sub>, was 2–5 events/(d · kg · keV) without applying a veto trigger.  
.....

Subject Index      F40, F41

# 1 Introduction

## 1.1 *Present status of dark matter search*

Dark matter (DM) is one of the important subjects in both cosmology and particle physics. Observations of the cosmic microwave background have shown that the DM accounts for 26.4% of the total energy density of the universe [1, 2]. A new physics theory beyond the Standard Model has to be developed. We expect that direct detection of DM may accelerate the progress on the theoretical front as well. Weakly Interacting Massive Particles (WIMPs) remain one of the most important candidates for DM. Lighter WIMPs on the order of sub-GeV have recently been proposed making low-energy, low-background detectors essential for WIMP searches [3].

At present, the most sensitive DM detector in the world is the XENONnT experiment using 8.5 tons of liquid Xe [4]. Attempts to verify annual modulation of the signal using NaI(Tl) detectors led to contradiction results. The annual modulation of the signal reported by the DAMA/LIBRA group [5] has not been confirmed by other groups operating similar NaI(Tl) detectors. As it stands, the ANAIS group ruled out the possibility of annual modulation [6], while the COSINE group reported annual modulation in the opposite phase [7] through DAMA-like analysis. It is essential to mention that concentrations of impurities causing the background at the region of interest were high for all experiments exploiting NaI(Tl) detectors. Even the DAMA/LIBRA experiment, that reported the highest sensitivity with NaI(Tl) detectors, has background about 6 orders of magnitude higher than those of the XENONnT experiment.

## 1.2 *PICOLON experiment*

The main background (BG) sources in NaI(Tl) crystals are  $^{40}\text{K}$  ( $^{\text{nat}}\text{K}$ ),  $^{232}\text{Th}$  (Th-series),  $^{226}\text{Ra}$  and  $^{210}\text{Pb}$  (U-series). In particular,  $^{40}\text{K}$  and  $^{232}\text{Th}$  are the main BG contributors at energies below  $100 \text{ keV}_{\text{ee}}$ , where  $\text{keV}_{\text{ee}}$  is an observed energy that is calibrated by electron energy.

PICOLON (Pure Inorganic Crystal Observatory for LOw-energy Neut(ra)rino) is a project designed for DM search using ultra high-purity NaI(Tl) detectors. Understanding of the nature of annual modulations reported by the DAMA/LIBRA group is one of the PICOLON objectives. Table 1 shows the concentrations of radioactive impurities (RIs) in the NaI(Tl) crystals used by DAMA/LIBRA, COSINE, ANAIS-112, SABRE, and PICOLON experiments. In 2020, we developed a ultra high-purity NaI(Tl) crystal named Ingot #85 using an optimized purification method that includes recrystallization and use of resins. Recently, we produced new NaI(Tl) crystal, called Ingot #94, using the same purification

**Table 1** Concentration of RIs and BG rate reported by DM experiments using NaI(Tl) crystals. The unit of dru stands for events/(d · kg · keV).

RIs	DAMA/LIBRA [8]	COSINE [9]	ANAIS-112 [6, 10]	SABRE [11, 12]	Ingot #85 [13]	Our goal
$^{nat}\text{K}$ [ $\mu\text{Bq/kg}$ ]	< 600	< 1060	545–1200	120	–	600
$^{232}\text{Th}$ [ $\mu\text{Bq/kg}$ ]	2–31	2.5–35	4	0.8	1.2±1.4	10
$^{226}\text{Ra}$ [ $\mu\text{Bq/kg}$ ]	8.7–124	11–451	10	5	13±4	10
$^{210}\text{Pb}$ [ $\mu\text{Bq/kg}$ ]	5–30	10–3000	740–3150	360	<5.7	50
BG rate (dru)	1	3	3.605±0.003	1.39±0.02	–	1

method as for Ingot #85. We will discuss the experimental setup and data acquisition system (DAQ) in Sect. 2. The BG analysis, energy calibration and noise reduction method are explained in Sect. 3.

## 2 Experimental setup

### 2.1 Detector and shielding

We assembled two detector modules using NaI(Tl) crystals Ingot #85 and #94. The cylindrical crystals have a diameter of 76.2 mm and a length of 76.2 mm. The bottom and side surfaces of the crystals were covered with Enhanced Specular Reflector Films (ESR™) to guide scintillation photons into optical window. The crystal was encapsulated into an acrylic housing and sealed with a 1cm-thick optical window of synthetic quartz. The assembled NaI(Tl) crystal was viewed by a 3-inch low BG Hamamatsu R11065-20 photomultiplier tube (PMT). The voltage divider circuits, for PMTs were optimized to reduce the distortion of large amplitude pulses, as shown in Fig. 1.

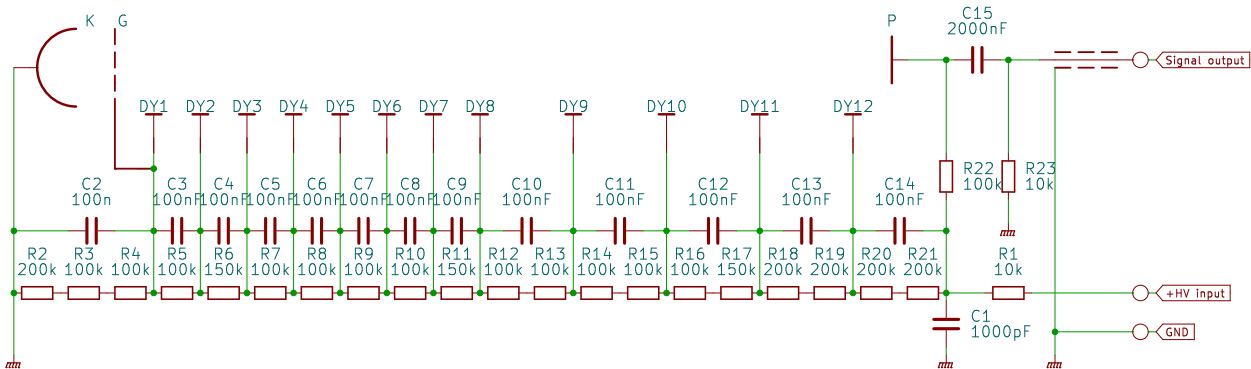


**Fig. 1** Optimized voltage divider circuits for Hamamatsu R11065-20 PMTs.

The experimental site is located at the KamLAND facility in Kamioka underground laboratory at 2700 m.w.e., where m.w.e. stands for meter water equivalent. Ingots #85 and #94 were installed into the shielding made of 5 cm thick oxygen-free copper blocks and 15 cm thick low-activity lead blocks. The concentration of radon in laboratory air is 20–50 Bq/m<sup>3</sup>. Therefore, we continuously supplied a pure nitrogen gas into the shield to purge out radon.

## 2.2 Data acquisition system

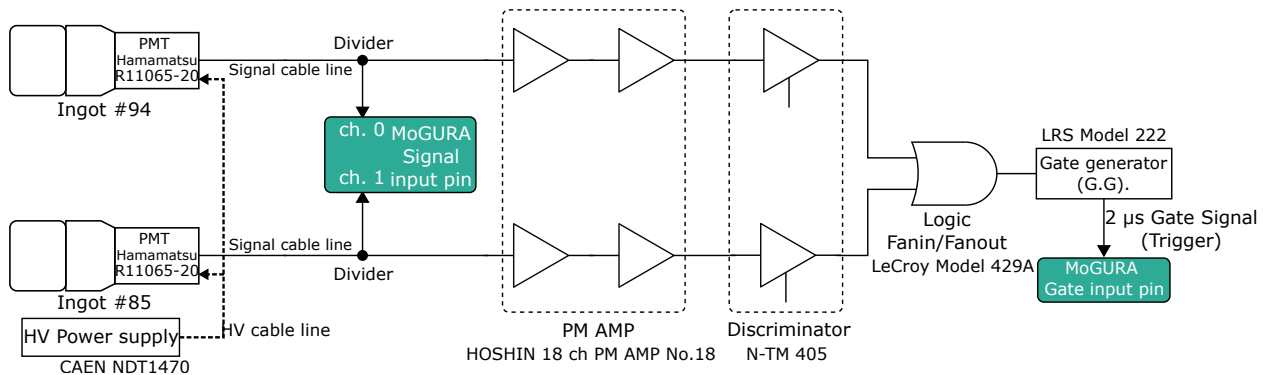


**Fig. 2** Schematic drawing of DAQ system.

A block diagram of trigger generation and data acquisition (DAQ) system is shown in Fig. 2. Signals from two PMTs produce a trigger for the DAQ without any external veto signal. The logic signals generated from both detectors create a trigger of DAQ. A long gate signal of 2  $\mu$ s is supplied to the gate input of MoGURA electronic board [14] to avoid a re-triggering.

## 3 Analysis

### 3.1 Energy calibration

Energy calibration of NaI(Tl) detectors was performed using <sup>133</sup>Ba, <sup>137</sup>Cs, and <sup>60</sup>Co standard sources. Figure 3 shows resulting calibration curves. Due to a non-linearity of a scintillation response in NaI(Tl), we calibrated energy regions below and above 100 keV separately. The region below 100 keV was calibrated using 6.4 keV, 31 keV, and 81 keV peaks from the <sup>133</sup>Ba source. The 6.4 keV peak from the <sup>133</sup>Ba source is created in a two step process. First, 34.9 or 35.8 keV  $K_{\beta}$  X-rays from electron capture in <sup>133</sup>Ba cause a photoelectric effect on an iodine atom located near the surface of the crystal. Second, the resulting iodine ion emits  $K_{\alpha}$  X-rays (28.6, 28.3 keV) that escape the sodium iodine crystal.

As a result, about 6 keV of energy remains inside the NaI(Tl) crystal. The energy region above 100 keV is calibrated using 303 keV and 356 keV gamma lines of  $^{133}\text{Ba}$ , and gamma lines from  $^{137}\text{Cs}$  and  $^{60}\text{Co}$ .

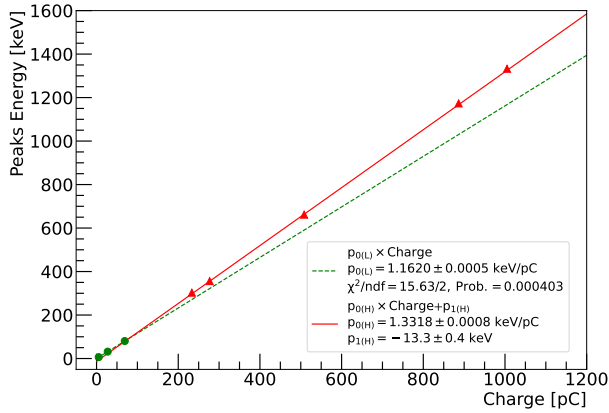


**Fig. 3** The energy calibration of NaI(Tl) detectors using  $^{133}\text{Ba}$ ,  $^{137}\text{Cs}$ , and  $^{60}\text{Co}$  sources. Two different fit functions were used for energy region below (dashed green) and above (solid red) 100 keV.

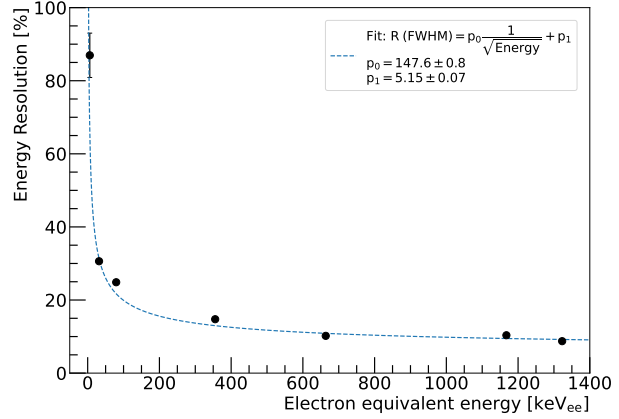


**Fig. 4** The energy resolution as a function of energy measured with the NaI(Tl) scintillating crystals.

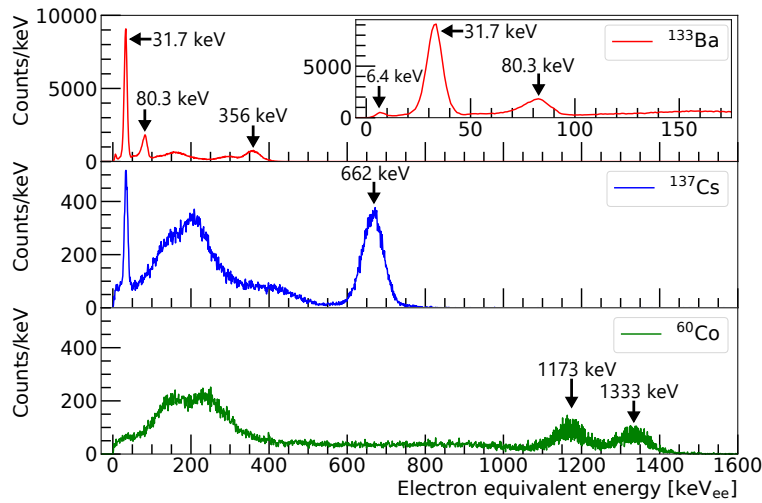


**Fig. 5** Energy spectra of  $^{133}\text{Ba}$  (top),  $^{137}\text{Cs}$  (middle), and  $^{60}\text{Co}$  (bottom) sources measured with the NaI(Tl) scintillating crystals.

Figure 4 shows the energy dependence of the energy resolution  $R(\%)$ , defined as

$$R(\%) = \frac{\Delta E}{E_0} \times 100, \quad (1)$$

where  $\Delta E$  is a full width at half maximum (FWHM) and  $E_0$  is the energy of a  $\gamma$ -ray. We fitted these data by  $R = p_0 \frac{1}{\sqrt{E_{ee}}} + p_1$  function. Figure 5 shows energy spectra for three standard sources.

### 3.2 Pulse-shape discrimination between $\alpha$ -rays and $\gamma$ -rays

The difference in pulse shapes allows us to discriminate  $\beta/\gamma$ -rays events from those induced by  $\alpha$ -rays. We applied Pulse Shape Discrimination (PSD) to distinguish events caused by  $\alpha$ -ray from all other events. Figure 6 shows a typical pulses of  $\alpha$ -rays and  $\beta/\gamma$ -rays [15]. The pulse-shape parameter named  $R_{\text{PSD}}$  is defined as a ratio of integrated currents over two different time windows after the pulse starts:

$$R_{\text{PSD}} \equiv \frac{Q_{\text{Part}}}{Q_{\text{Total}}} = \frac{\int_{200 \text{ ns}}^{1200 \text{ ns}} I(t) dt}{\int_0^{1200 \text{ ns}} I(t) dt} \quad (2)$$

where  $I(t)$  is the current pulse,  $Q_{\text{Total}}$  and  $Q_{\text{Part}}$  are the integrated charges over two different time intervals since pulse start:  $[0 \text{ ns}, 1200 \text{ ns}]$  for  $Q_{\text{Total}}$ ,  $[200 \text{ ns}, 1200 \text{ ns}]$  for  $Q_{\text{Part}}$ .

Figure 7 shows the scatter plot of the electron equivalent energy versus  $R_{\text{PSD}}$ . We selected a  $R_{\text{PSD}}$  threshold to be 0.52 to achieve a clear separation between  $\alpha$ -rays and  $\beta/\gamma$ -ray events. The resulting spectra of the  $\alpha$ -rays events and  $\beta/\gamma$ -rays events shown in Fig. 8 after applying the PSD selection cut. The PSD selection is valid in the region between 1200 to 6000  $\text{keV}_{ee}$  where  $\beta/\gamma$ -ray events do not mix with the  $\alpha$ -ray events spectrum.

### 3.3 Low energy region analysis

To search for DM, we need to remove noise events in the low energy region below 100  $\text{keV}_{ee}$ . The Cherenkov radiation and dark current in PMTs generate a large number of noise pulses. We use two noise reduction methods: a single noise reduction to separate single-pulse noise from scintillation pulses; and the PSD noise reduction to remove noise events below 10  $\text{keV}_{ee}$ .

#### 3.3.1 Single pulse noise reduction

Figure 9 shows typical noise and scintillation pulses. The noise waveform consists of a single pulse followed by no pulse after 200 ns. In contrast, the scintillation signal consists of many pulses spread over the scintillation decay time. Therefore, the scintillation events are discriminated from all events using the timing window  $\Delta T > 200 \text{ ns}$  after the first pulse, where  $\Delta T$  is the time difference between two single pulses.

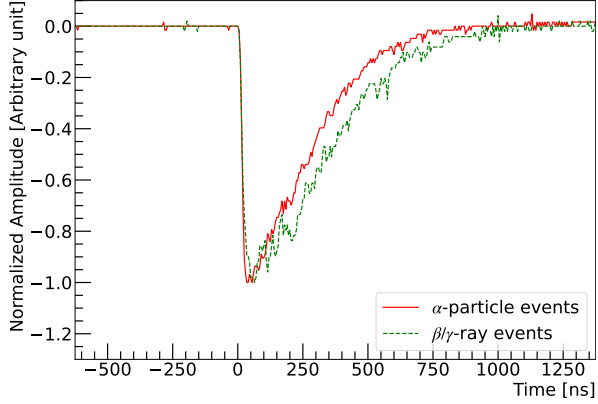


**Fig. 6** Typical signal waveforms of  $\alpha$ -rays and  $\beta/\gamma$ -rays measured with present NaI(Tl) scintillator [15].

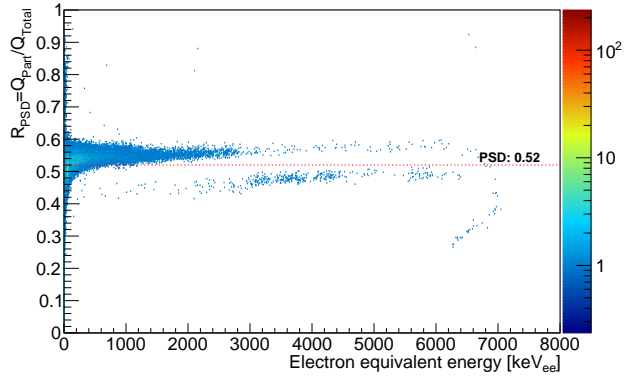


**Fig. 7** Scatter plot of the electron equivalent energy versus  $R_{\text{PSD}}$  for BG data accumulated using present NaI(Tl) detectors. We set  $R_{\text{PSD}} < 0.52$  as a threshold to separate  $\alpha$ -rays from  $\beta/\gamma$ -rays [15].

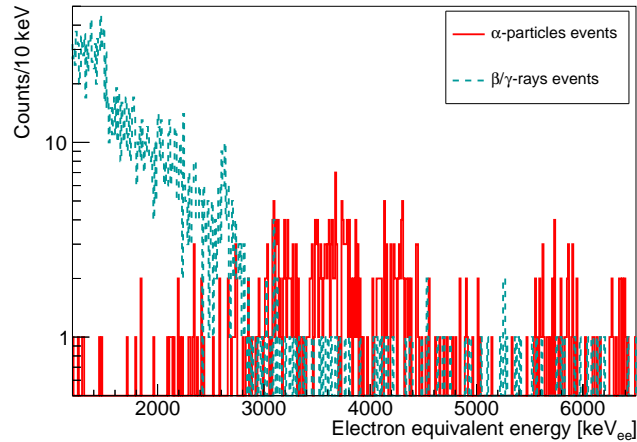


**Fig. 8** Energy spectrum with  $\alpha$ -rays events (red solid) or  $\beta/\gamma$ -rays events (blue dashed) [15].

### 3.3.2 PSD noise reduction

We applied a simple noise threshold to the PSD scatter plot in Fig. 7 to reject PMT noise events below 10 keV<sub>ee</sub>. A magnified part of the Fig. 7 is shown in Fig. 10 using a logarithmic scale. One can see two clearly separated event distributions below 100 keV<sub>ee</sub>. We investigated noise events with energy lower than 100 keV<sub>ee</sub> and  $R_{\text{PSD}} > 0.64$ . A typical waveform for such events is shown in Fig. 11, confirming that those events are noise pulse from PMTs. In addition, Noise signals from VME bus traffic and power lines cause the baseline

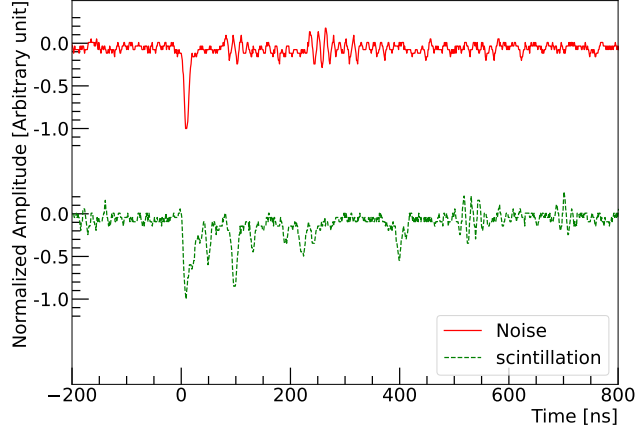


**Fig. 9** Example of waveform at 3 keV<sub>ee</sub> signals. Top: single pulse noise event signal. Bottom: NaI(Tl) scintillation event signal.

instability. Consequently, the  $R_{\text{PSD}}$  increases and we can remove these events from Fig. 10. Figure 12 shows the energy spectrum before and after applying two reduction methods. The effect of noise reduction is clearly seen. However, we have to admit that the peak around 3 keV<sub>ee</sub> is caused by insufficiency of the simple PSD reduction methods.

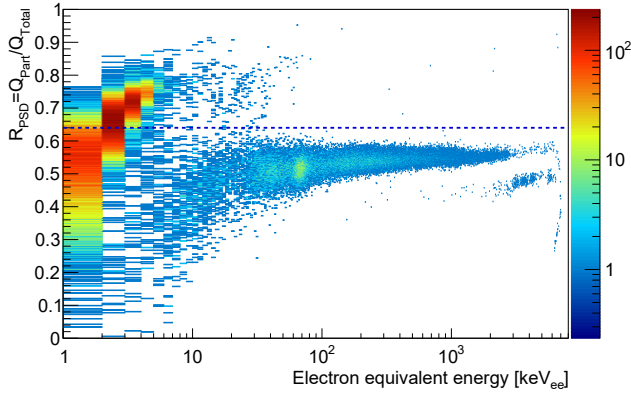


**Fig. 10** Scatter plot for low-energy PSD.

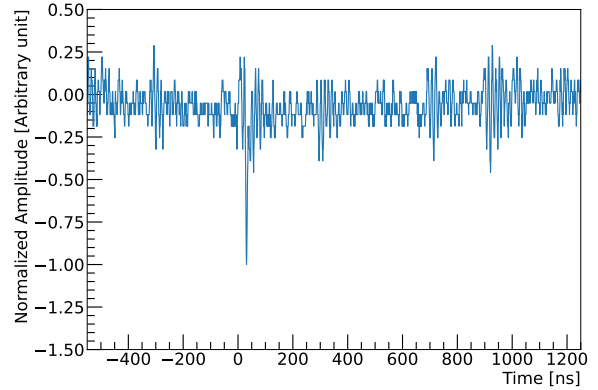


**Fig. 11** typical waveform of noise event ( $R_{\text{PSD}} > 0.64$ ) on scatter plot for low-energy PSD.

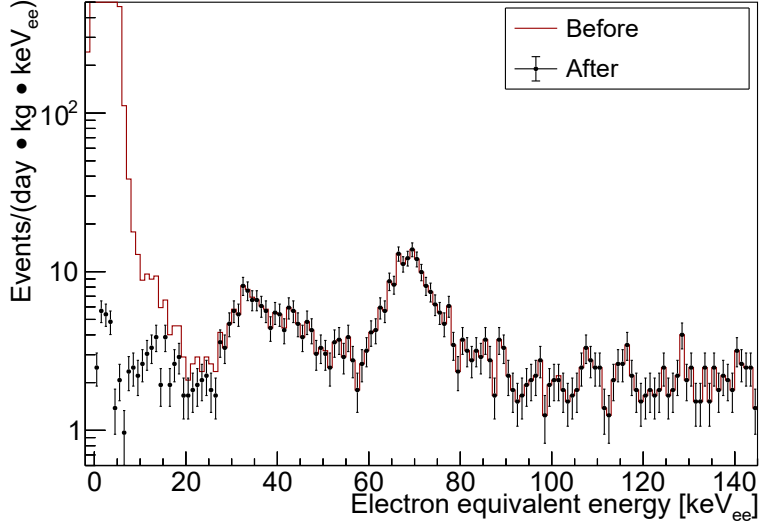


**Fig. 12** Low-energy BG spectra before (red line) and after (black dots) noise reduction acquired using NaI(Tl) detectors. The live time was 5.39 days $\times$ 1.34 kg.

## 4 Result

### 4.1 Concentration of radioactive impurities in Ingot #94

We extracted  $\alpha$ -rays by PSD analysis. The energy spectrum of  $\alpha$ -rays is shown in Fig. 13. We found 5 prominent peaks between 3000 keV<sub>ee</sub> and 6000 keV<sub>ee</sub>, which consist of  $\alpha$ -rays from U-series and Th-series. We analyzed each RI in the prominent peaks as shown in Table 2. Closely located peaks are combined into one peak. For example, two peaks (index A in Table 2) of  $^{238}\text{U}$  (U-series) and  $^{232}\text{Th}$  (Th-series) cannot be resolved due to the low energy resolution.

**Table 2** RI events with alpha-ray in Ingot #94.

Index	RIs	Energy Range [keV <sub>ee</sub> ]	Events
A	$^{238}\text{U}(\text{U}) + ^{232}\text{Th}(\text{Th})$	2210–2900	33 $\pm$ 6
B	$^{234}\text{U}(\text{U}) + ^{230}\text{Th}(\text{U}) + ^{226}\text{Ra}(\text{U})$	2950–3350	72 $\pm$ 9
C	$^{228}\text{Th}(\text{Th}) + ^{224}\text{Ra}^*(\text{Th}) + ^{222}\text{Rn}(\text{U}) + ^{210}\text{Po}(\text{U})$	3380–3970	118 $\pm$ 11
D	$^{218}\text{Po}(\text{U}) + ^{212}\text{Bi}(\text{Th}) + ^{224}\text{Ra}^*(\text{Th}) + ^{220}\text{Rn}(\text{Th})$	4000–4480	71 $\pm$ 9
E	$^{216}\text{Po}(\text{Th})$	4690–5150	15 $\pm$ 4

The RI concentration  $C_{\text{RI}}$  [Bq/kg] was calculated using the formula

$$C_{\text{RI}} = \frac{N}{tM} \pm \frac{\sigma_N}{tM}, \quad (3)$$

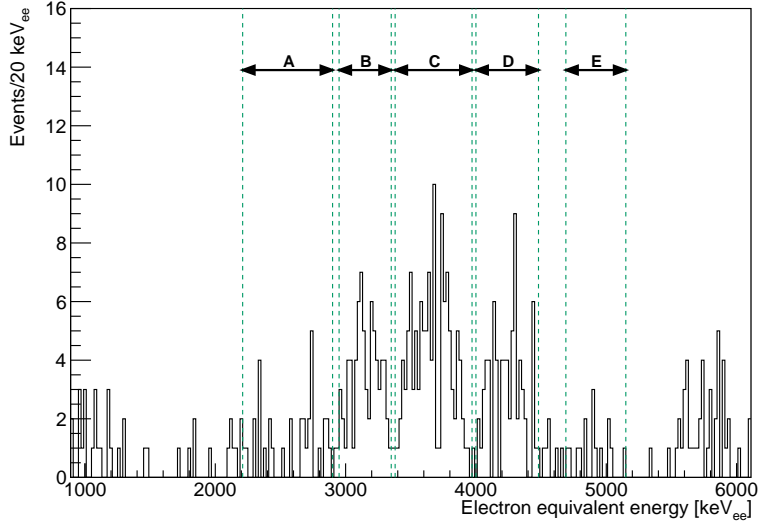


**Fig. 13**  $\alpha$ -ray spectrum between about 1000 to 6000 keV<sub>ee</sub>.

where  $N$  and  $\sigma_N$  are number of RI events and statistical error,  $t$  is livetime and  $M$  is the mass of NaI(Tl) crystal. For the Ingot #94, the exposure is  $t \times M = 28.26$  days  $\times$  1.34 kg. The concentrations of RI are shown in Table 3. The NaI(Tl) crystal Ingot #94 was confirmed

**Table 3** Concentration of RIs in Ingot #94.

RI	Ingot #94	Our goal	DAMA/LIBRA [8]
$^{232}\text{Th}$ [ $\mu\text{Bq/kg}$ ]	$4.6 \pm 1.2$	$< 10$	2-31
$^{226}\text{Ra}$ [ $\mu\text{Bq/kg}$ ]	$7.9 \pm 4.4$	$< 10$	8.7-124
$^{210}\text{Pb}$ [ $\mu\text{Bq/kg}$ ]	$19 \pm 6$	$< 50$	5-30

to be highly radiopure with RI activity equivalent to DAMA/LIBRA crystals.

#### 4.2 The low energy region

There were many intense peaks from  $^{126,125}\text{I}$ ,  $^{210}\text{Pb}$  and  $^{40}\text{K}$  below 100 keV<sub>ee</sub>. We investigated temporal variation of the BG at low energies. Figure 14 shows the variation of some peaks  $^{126}\text{I}$  (35 keV  $K_\alpha$  X-ray, half-time  $T_{1/2} = 12.5$  d),  $^{210}\text{Pb}$  (46.5 keV  $\gamma$ -ray,  $T_{1/2} = 22.2$  y) and the  $^{125}\text{I}$  (64 keV  $\gamma$ -ray,  $T_{1/2} = 59.4$  d) energy spectrum (red histogram). The iodine peaks quickly diminished after 42.31 days of data taking (black histogram). The temporal variation of the BG rate is shown in Fig. 15. The spectra were fitted to the three peaks composed of superposition of three Gaussians and constant terms. Although, we have no

data from 7.4 to 21.4 days due to a HV hardware malfunction, we obtained a clear time dependence of the BG rate.

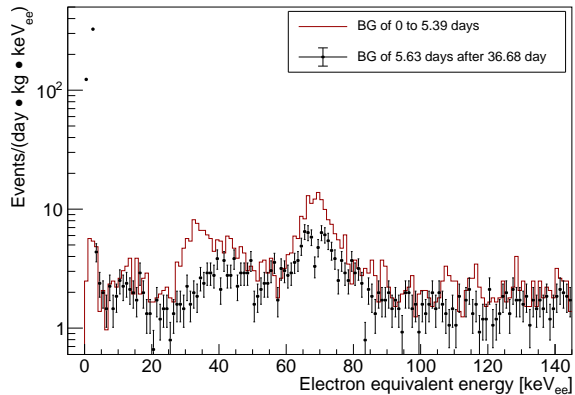


**Fig. 14** The earlier low energy spectrum (red line) were accumulated during first 5.4 days of measurements, and the later low energy spectrum (black point) was taken for 5.6 days of measurements after 36.7 days of installation.

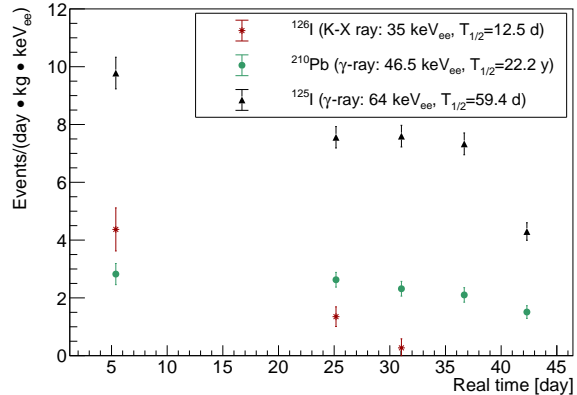


**Fig. 15** Temporal variation of RI concentration in Ingot #94.

## 5 The detector sensitivity

The expected sensitivity of the Ingot #94 detector in the absence of the annual modulation was estimated from the BG spectra. A flat BG was assumed for the first 5.4 days of

**Table 4** The BG rate of Ingot #94 crystal in several energy regions.

Energy region [keV <sub>ee</sub> ]	BG rate	Upper limit of BG error
	[events/(d · kg · keV)]	
[2, 6] (all)	$3.42 \pm 0.35$	0.94
[2, 4] (noisy)	$5.12 \pm 0.73$	0.94
[4, 6] (not noisy)	$1.73 \pm 0.63$	0.80

the BG spectra (red line spectra in Fig. 14), because the BG decreases with time, conversely there is an excess of events due to noise around 3 keV<sub>ee</sub>. The flat background is calculated for three energy regions as shown in Table 4. The sensitivity of the Ingot #94 detector is calculated using the [4, 6] keV<sub>ee</sub> (not noisy) BG rate. From the flat BG, the expected event

rate was calculated to obtain an upper limit of 90% C.L. with Poisson statistics. Figure 16 shows the sensitivity to spin-independent (SI) DM interaction for Ingot #94 (red solid line). The solid red line is the upper limit of BG for the Ingot #94 crystal that partially covers the search region of the DAMA/LIBRA experiment. The red dashed line is a simulation of the case where 400 kg of NaI(Tl) crystals with BG equivalent to Ingot #94 are prepared and measured for one year, which completely covers the search of the DAMA/LIBRA experiment.

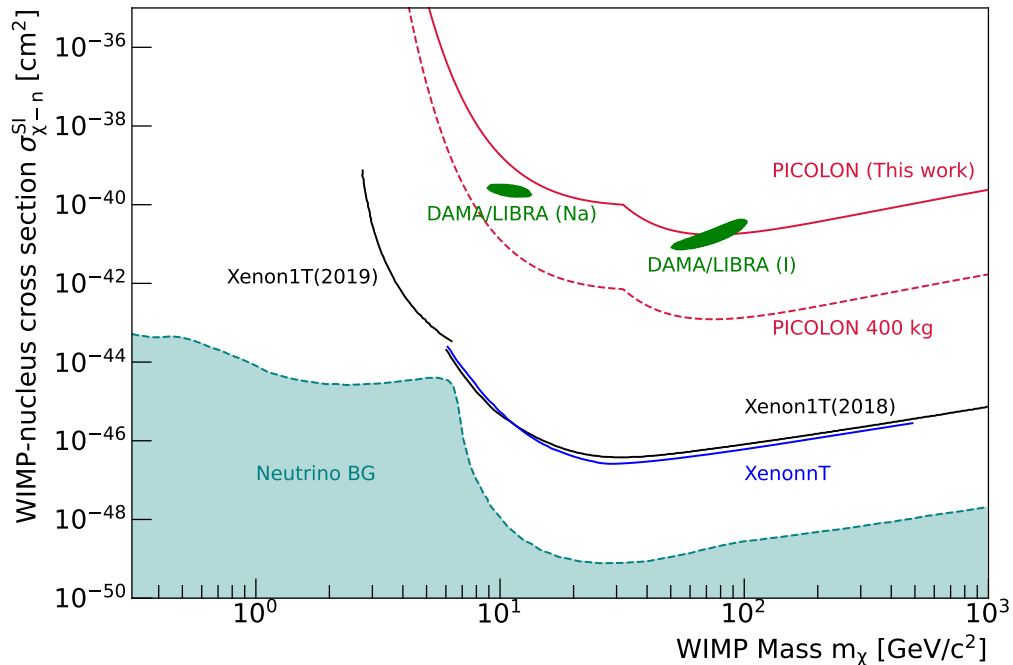


**Fig. 16** The detector sensitivity [3, 4, 16].

## 6 Summary and remarks

We have developed high-purity NaI(Tl) crystals with the radiopurity similar to that of the DAMA/LIBRA crystals, and confirmed the reproducibility of the crystal purification method. A BG reduction of about one order of magnitude would be necessary for verification of the DAMA/LIBRA result, which is one of the objectives of the PICOLON project. The present detector is comparable sensitivity to the DAMA/LIBRA crystals. We will construct a DM search apparatus that is able to cover the DAMA/LIBRA DM search area using 400 kg ultra high-purity NaI(Tl) crystals with a BGs similar to those of the Ingot #94 crystal [17]. We will also optimize the BG and noise reduction methods.

## Acknowledgments

This work was supported by JSPS KAKENHI (Grant Nos.: 26104008, 19H00688, and 20H05246), a discretionary expense of the president of Tokushima University, and the World Premier International Research Center Initiative (WPI Initiative).

## References

- [1] N. Aghanim et al., *A&A*, **641**, A1 (2020).
- [2] N. Aghanim et al., *A&A*, **641**, A6 (2020).
- [3] R. L. Workman et al., *PTEP*, **2022**(8), 083C01 (2022).
- [4] E. Aprile et al., *Phys. Rev. Lett.*, **131**, 041003 (2023).
- [5] R. Bernabei et al., *SciPost Phys. Proc.*, page 025 (2023).
- [6] J. Amaré et al., *Phys. Rev. D*, **103**, 102005 (2021).
- [7] G. Adhikari et al., *Scientific Reports*, **13**, 4676 (2023).
- [8] R. Bernabei et al., *Nucl. Instr. and Methods in Phys. Res. Sect. A*, **592**(3), 297–315 (2008).
- [9] B. J. Park et al., *Eur. Phys. J. C*, **80**, 814 (2020).
- [10] J. Amaré et al., *Eur. Phys. J. C*, **79**, 412 (2019).
- [11] F. Calaprice et al., *Eur. Phys. J. C*, **82**, 1158 (2022).
- [12] A. Mariani et al., *Journal of Physics: Conference Series*, **2156**, 012022 (2022).
- [13] K. Fushimi et al., *PTEP*, **2021**(4), 043F01 (2021).
- [14] A. Terashima et al., *Journal of Physics: Conference Series*, **120**, 052029 (2008).
- [15] K. Kotera et al., *KEK Proceedings, Radiation Detectors and Their Uses, 37th Workshop* (to be published, in Japanese) (2023).
- [16] E. Aprile et al., *J. Cosmol. Astropart. Phys.*, **2016**(04), 027 (2016).
- [17] K. Fushimi et al., *KEK Proceedings, Radiation Detectors and Their Uses, 37th Workshop* (to be published) (2023).